JOURNAL OF VIROLOGY, June 2005, p. 8032–8045 Vol. 79, No. 13
0022-538X/05/$08.00+0 doi:10.1128/JVI.79.13.8032–8045.2005

Investigation by Atomic Force Microscopy of the Structure of Ty3 Retrotransposon Particles

Yurii G. Kuznetsov,[1]† Min Zhang,[2]† Thomas M. Menees,[3] Alexander McPherson,[1] and Suzanne Sandmeyer[2]*

Departments of Molecular Biology and Biochemistry[1] and Biological Chemistry,[2] University of California, Irvine, California 92697, and Division of Cell Biology and Biophysics, University of Missouri, Kansas City, Missouri[3]

Received 6 December 2004/Accepted 16 March 2005

Ty3, a member of the *Metaviridiae* family of long-terminal-repeat retrotransposons found in *Saccharomyces cerevisiae*, encodes homologs of retroviral Gag and Gag-Pol proteins, which, together with genomic RNA, assemble into virus-like particles (VLPs) that undergo processing and reverse transcription. The Ty3 structural proteins, capsid and nucleocapsid, contain major homology and nucleocapsid motifs similar to retrovirus capsid and nucleocapsid proteins, but Ty3 lacks a matrix-like structural domain amino terminal to capsid. Mass spectrometry analysis of Ty3 Gag3 processing products defined an acetylated Ser residue as the amino terminus of Gag3/p34, p27, and CA/p24 species and supported a model where p34 and p27 occur in phosphorylated forms. Using atomic force microscopy, VLPs were imaged from cells producing wild-type and protease and reverse transcriptase mutant Ty3. Wild-type VLPs were found to have a broad range of diameters, but the majority, if not all of the particles, exhibited arrangements of capsomeres on their surfaces which were consistent with icosahedral symmetry. Wild-type particles were in the range of 25 to 52 nm in diameter, with particles in the 42- to 52-nm diameter range consistent with T=7 symmetry. Both classes of mutant VLPs fell into a narrower range of 44 to 53 nm in diameter and appeared to be consistent with T=7 icosahedral symmetry. The smaller particles in the wild-type population likely correspond to VLPs that have progressed to reverse transcription or later stages, which do not occur in the protease and reverse transcriptase mutants. Ty3 VLPs did not undergo major external rearrangements during proteolytic maturation.

This study was undertaken to investigate the virus-like particle (VLP) structure of the long-terminal-repeat (LTR) retrovirus like element Ty3 from *Saccharomyces cerevisiae* (75). The retrotransposon VLP is analogous to the nonenveloped core particle of retroviruses. Determination of detailed structures of retroviral cores is complicated, because cores are enveloped and heterogeneous and mature particles of many retroviruses are relatively fragile (20, 79). It was of interest to determine whether the smaller size of the Ty3 structural domain would be reflected in a simplification of particle morphology. Retroviral cores are initially assembled from Gag together with lesser amounts of Gag-Pol to form spherical, immature cores. Naked (nonenveloped) cores range in average diameter from 79 nm for Rous sarcoma virus (RSV) (38) to 96 nm for murine leukemia virus (MLV) (86). Human immunodeficiency type 1 (HIV-1) cores assembled in vitro from ΔMA CA-NC-Δ p6 are about 112 nm in diameter and, similar to immature cores, are spherical (84). Analysis of viral cores assembled from Gag in vitro or of immature cores isolated from infected cells indicates that Gag is arrayed amino to carboxy terminal, radially from outer to inner portion of the particle (8, 21, 84, 86, 88). Spherical, immature cores do not appear to have icosahedral organization (21, 83, 86). However, HIV (7, 49, 62) and MLV (86) particles comprised of Gag display p6 lattice structure.

Retroviral cores mature by proteolytic cleavage of Gag into structural species including matrix (MA), capsid (CA), and nucleocapsid (NC) as viruses bud from the host cell (13). During formation of the mature core, CA is freed from its MA-mediated membrane association and condenses into a characteristic shell. For example, alpha and gamma retroviruses have roughly spherical or polygonal cores, whereas lentiviruses have cone-shaped cores. Where it is understood at the molecular level, this change in particle shape is accompanied by structural changes in CA itself. Studies of RSV (34) and HIV-1 CA (27, 80) proteins have shown that CA assembled in the context of amino-terminal extensions (mimicking the unprocessed Gag context) is constrained, resulting in spherical particles in vitro and immature morphology in vivo. Crystal structures of RSV and HIV-1 CA proteins have further elucidated the molecular basis of this structural switch. The processed CA amino terminus in the mature particles interacts with internal residues in a salt bridge which stabilizes a CA structure that is not possible in the context of an amino-terminal extension (22, 26, 59, 80).

Cryoelectron microscopy (cEM) of two-dimensional (2D) arrays of HIV-1 (24, 49), MLV (23, 55, 90, 91), and RSV (37, 54) CA and X-ray crystal structure analysis of MLV CA (60) indicate that CA subunits form hexagonal clusters which might serve as capsomeres in an icosahedral particle (19). In the case of HIV-1, it has been proposed that core particles are not icosahedral but that CA in the mature core is arranged with local symmetry. HIV-1 assembled in vitro assumes cone shapes consistent with a distribution of pentagonal vertices in a closed, helical hexagonal net describing a fullerene cone (24, 49). HIV-1 CA assembled in vitro also forms tubes composed of

* Corresponding author. Mailing address: Department of Biological Chemistry, D2402688 Med Sci-I, University of California, Irvine, CA 92697-1700. Phone: (949) 824-7571. Fax: (949) 824-7571. E-mail: sbsandme@uci.edu.

† These authors contributed equally to this work.

hexameric rings consistent with this model (49). Particles composed of hexameric arrangements of CA and having cone angles allowed by the fullerene cone model have now been imaged in mature HIV-1 cones by cEM (9). Nonetheless, the heterogeneous shapes of particles of other retroviruses cannot be as readily reconciled with rigorous icosahedral symmetry. Description of these nonstandard structures is complicated by the fact that the presumably irregularly spaced pentons which would close irregular structures cannot be imaged by methods that require molecular averaging (38, 82, 86).

The genomes of metaviruses, including Ty3, are organized similarly to retrovirus genomes but are simpler (48, 75, 77). Ty3 encodes Gag3 and Gag3-Pol3 polyproteins from which major structural proteins CA and NC and catalytic proteins, protease (PR), reverse transcriptase (RT), and integrase (IN), respectively, are produced (28, 29). One appealing feature of the Ty3 model system is its relatively simple Gag3 major structural domain. Ty3 Gag3 is 290 amino acids (aa) in length. It is processed into species previously described based on gel mobility as 31-kDa, 26-kDa (CA), and 9-kDa (NC) proteins (40, 66). Gag3 is expressed at approximately a 20-fold higher level than Gag3-Pol3, which is produced through a programmed translational frameshift (18, 41). Although Ty3 CA primary sequence does not show obvious long-range similarity to retroviral CA, it does contain the major homology region (MHR) which is conserved among retrovirus CA proteins, and mutations in this domain are associated with similar replication phenotypes as have been observed for retrovirus MHR mutants (15, 65). Ty3 NC is a 57-aa protein and contains one copy of a $CX_2CX_4HX_4C$ zinc-binding domain (66). It is also essential for proper particle maturation. Ty3 Gag3 and Gag3-Pol3 and RNA form intracellular VLPs, which undergo processing followed by reverse transcription (28). Consistent with an intracellular life cycle, Ty3 does not encode membrane-associated envelope (Env) or MA domains.

Transmission EM of the Ty3 particle indicates that it is approximately 50 nm in diameter (28). Although no detailed structure has been determined for Ty3 particles, they are functionally analogous to nonenveloped retrovirus cores and to VLPs formed by other retrotransposons (14). Retroviruses and metaviruses, such as Ty3, are more distantly related to pseudoviruses, such as Ty1 (5, 81). In the case of Ty1, the *TYA* reading frame encodes a 440-aa protein, p1, which is processed into a 408-aa (p2) major structural protein and smaller species (25, 53, 87). Expression of full-length Ty1 results in accumulation of particles of variable shape ranging from 30 to 78 nm in diameter. This variability precluded analysis of wild-type (wt) VLPs by methods which rely on molecular averaging (10). However, expression of *TYA* which encodes the full-length 440-aa major capsid protein and truncated variants as short as 346 aa resulted in more regular particles that have been studied by transmission and cEM (1, 10, 67). These studies showed that particles could be described in terms of icosahedral symmetry and represented a series from T=3 to T=9, where T and particle diameter correlated roughly with the length of capsid protein expressed.

In the current study, the molecular structure of Ty3 particles was examined for the first time. Atomic force microscopy (AFM) was used to determine whether Ty3 particles have ordered structure and how that structure is affected by the proteolytic processing and reverse transcription. The advantages of AFM are that particles can be visualized in a fully hydrated state, surface morphology is evident because the images are not projections of entire particles, and individual particles are recorded. The last point is particularly important if significant morphological differences exist between individuals, as variable features would be underexplored in approaches that rely on reconstructions using symmetry averaging. Particles from cells expressing Ty3 wt and PR and RT mutants displayed an ordered structure consistent with icosahedral symmetry. The largest of the wt particles resembled the particles observed in cells expressing the PR or the RT mutants. However, expression of wt Ty3 was also associated with the presence of smaller, ordered particles, suggesting that reverse transcription, but not PR processing, is associated with major external reorganization of the particle. The stability of the Ty3 particles and the degree of order we observed suggest that Ty3 is a useful model for understanding aspects of the relationship between virus particle structure and function.

MATERIALS AND METHODS

Yeast and bacterial strains and culture conditions. *Escherichia coli* and *S. cerevisiae* cells were cultured and transformed by standard methods (2). All plasmids were amplified in *E. coli* HB101 (F^- *hsdS20* [r_B^- m_B^-] *recA13 leuB6 ara-14 proA2 lacY1 galK2 rpsL20* [sm^r] *xyl-5 mtl-1 supE44*Δ). AGY-9 (*MAT***a** *ura3-52 his4-539 lys2-801 trp1-*Δ*63 leu2-*Δ*1 spt3-202*) (a gift from J. D. Boeke, The Johns Hopkins University) was used to produce Ty3 particles. This strain was grown at 37°C for several generations in order to attempt to reduce the occurrence of background particles in the VLP fraction. The pDLC201 (pEGTy3-1) (29) and Ty3 mutant derivatives described below were expressed in AGY-9. Strain TMY43 (*MAT***a** *ura3-52 trp1-H3 his3-*Δ*200 ade2-101 lys2-1 leu1-12 can1-100 bar1*::*hisG spt3*Δ*202* Ty3 null) was used for mass spectrometry analysis of Ty3 Gag3 and its derivatives. Transformed cells were isolated on synthetic media containing 2% dextrose as a carbon source (SD-ura). For galactose induced expression of Ty3 for VLP preparation and immunoblot analysis, cultures were grown to log phase (optical density at 600 nm [OD_{600}] = 0.25 to 0.35) in synthetic media containing 1% raffinose (SR-ura) and induced by addition of galactose to 2% (SG-ura). Cells were grown for 24 h at 28°C.

Plasmids. wt Ty3 was expressed from pDLC201 (29). This is a high-copy, *URA3*-marked plasmid. It contains the *GAL1-10* upstream activating sequence fused at nucleotide position 123 of the Ty3 upstream LTR so that Ty3 expression is induced by growth in galactose. The Ty3 PR and RT mutants were both derived by mutagenesis of pDLC201. The Ty3 expressed from plasmid pJK776 with the mutation (D59I) at the catalytic site of Ty3 PR was defective in proteolysis (40). The Ty3 expressed from plasmid pTy3RTD213N is modified within the RT coding sequence (D213N) and is defective in reverse transcription (personal communication with and generous gift from S. LeGrice and D. Lener, HIV Drug Resistance Program, National Cancer Institute, Frederick, MD).

VLP preparation. One-hundred-milliliter cultures of AGY-9 cells transformed with pEGTy3-1 or its derivatives, carrying Ty3 elements with mutations in conserved PR or RT residues, were grown to late log or stationary phase (A_{600} = 1.3 to 3.4) in SG-ura medium for 24 h to induce Ty3 expression. VLPs were prepared as previously described (28). Cells were harvested, washed, and digested with zymolyase. The spheroplasts, generated from zymolyase digestion, were lysed by vortexing with glass beads in VLP buffer B (9 mM HEPES [pH 7.8], 15 mM KCl, 5 mM $MgCl_2$) and fractionated over a 20/30/70% (542 μl, 253 μl, and 181 μl, respectively) sucrose step gradient by centrifugation in a TLS55 rotor in the Optima TL-100 ultracentrifuge (Beckman-Coulter, Fullerton, CA) at 86,000 × *g* for 68 min at 4°C. A total of 175 μl from the 70/30% interface of each gradient was collected. A 5-μl aliquot of the interface fraction was used for AFM imaging.

Immunoblot analysis. For immunoblot analysis the protein content of the VLP fraction was determined by Bradford assay (6). Five micrograms of whole-cell extract or 0.2 μg of concentrated VLP proteins was fractionated by electrophoresis on sodium dodecyl sulfate (SDS)–10% polyacrylamide gels. Proteins were transferred to Immobilon-P membranes (Millipore Corp., Bedford, MA) using a semidry transfer apparatus (Bio-Rad Inc., Hercules, CA). The immunoglobulin G (IgG) fraction of rabbit polyclonal anti-CA antisera (57) was prepared by affinity chromatography purification over protein A-agarose (Bio-Rad).

Blots were blocked in 2.5% nonfat milk-PBS-T (20 mM NaH_2PO_4, 80 mM Na_2HPO_4, 100 mM NaCl, 0.2% Tween 20) and incubated with rabbit polyclonal IgG against CA (1:10,000) (57). Immunoblots were washed with PBS-T, incubated with secondary antibodies to rabbit IgG conjugated to horseradish peroxidase (1:20,000), and washed again with PBS-T. Secondary antibodies to rabbit IgG were detected by chemiluminescence using the ECL system (Amersham Biosciences UK Ltd.).

Mass spectrometry. A VLP-enriched fraction was prepared as previously described from TMY43 cells expressing Ty3 (28). The VLP-enriched 30% to 70% interface fraction was further fractionated by 2D gel electrophoresis. Two-dimensional electrophoresis was performed according to the method of O'Farrell (64) by Kendrick Labs, Inc. (Madison, WI). Myosin (220,000), phosphorylase A (94,000), catalase (60,000), actin (43,000), carbonic anhydrase (29,000), and lysozyme (14,000) (Sigma Chemical Co., St. Louis, MO) were added as molecular weight standards to the agarose that sealed the isoelectric focusing (IEF) tube gel to the slab gel. These standards appeared as bands at the basic edge of the Coomassie brilliant blue R-250-stained 10% acrylamide slab gel or special silver-stained (63) 10% acrylamide slab gel. Gel spots were trypsinized in situ, and the peptides were eluted for mass spectrometric analysis. Matrix-assisted laser desorption deionization—mass spectrometry (MALDI-MS) was performed on tryptic peptides of the isolated p38, p31, and CA proteins by the Protein Chemistry Core Facility, HHMI/Columbia University College of Physicians and Surgeons, New York, N.Y., on a PerSeptive Voyager DE-RP mass spectrometer. Peptides were identified using ProFound (http://129.85.19.192/profound-bin/WebProFound.exe) and MS-Fit (http://prospector.ucsf.edu).

Atomic force microscopy. Five microliters of the Ty3 interface VLP fraction (protein concentration, 0.1 μg/μl to 0.15 μg/μl, except for the negative control, which was 0.06 μg/μl) was applied directly to a glass slide coated with poly-L-lysine and fixed by the addition of 1.0 μl of 25% glutaraldehyde (EM grade; Sigma Inc.). The particles adhered to the substrate and, though otherwise soft and deformable, were stable to probe tip pressure after this mild fixation. VLPs were scanned at 26°C using oxide-sharpened silicon nitride tips in a 75-μl fluid cell filled with buffer B. The images were collected using tapping mode (30, 31) with an oscillation frequency of 9.2 kHz and a scan frequency of 1 Hz. AFM procedures were fundamentally the same as described for previous investigations of retroviruses (43–45). The instrument used was a Nanoscope IIIa (VEECO, Santa Barbara, CA).

Because an image obtained from AFM represents the convolution of the cantilever tip shape, which is not infinitely sharp, lateral dimensions of objects can be significantly exaggerated. Vertical distances can be precise to less than 0.5 nm. Thus, the sizes of spherical or cylindrical objects are measured by their heights above background. However, the accuracy of this measurement depends upon the amount of interfering particulates deposited on the substrate. Center-to-center distances of objects in close packed arrays, such as the distances between vertices on the surface of an icosahedron, are also accurate and serve as appropriate dimension estimates. These measurements were calibrated using Chlorella virus PBCV-1, in which the capsomere-to-capsomere distance is known to be 7.0 nm (42).

RESULTS

Characterization of Ty3 major structural proteins. In order to better understand the structure of the VLP, further characterization of the processing products of Gag3 was undertaken. Expression of Ty3 from a promoter under control of the *GAL1-10* upstream activating sequence in plasmid pDLC201 results in VLP production and transposition (28, 29). At early times, only the precursor Gag3 and Gag3-Pol3 polyproteins are observed. Gag3 was designated p38 because it has the approximate mobility of a 38-kDa protein. After longer periods of Ty3 expression, CA and NC are produced by Ty3 PR processing of Gag3. A minor species with an apparent mobility of a protein of 31 kDa is also observed (data not shown). Previous analysis showed that the amino terminus of NC created by Ty3 PR processing is encoded at *GAG3* open reading frame (ORF) codon position 234 (40). (Although NC was originally designated p9 based on mobility, it will henceforth be designated p7 based on its mass.) In this report, positions are expressed relative to the *GAG3* ORF or Gag3 protein with position 1 the initiator Met codon or residue, respectively. The amino termini of Gag3, p31, and CA species are blocked and were refractory to Edman degradation analysis performed to determine amino termini of other Ty3 proteins (40). In order to physically define the major structural components of the Ty3 VLP, Gag3, p31, and CA were isolated using 2D gel electrophoresis and analyzed using mass spectrometry.

Yeast strain TMY43 was transformed with plasmid pDLC201, and transformants were selected on SD-ura. Cells were grown to log phase in SR-ura and induced for Ty3 expression by addition of galactose to 2% or were allowed to continue growing in SR-ura. As described previously (28), whole-cell extracts were fractionated on 20/30/70% sucrose step gradients to derive a VLP-enriched fraction. The 30/70% interface fraction was removed from the gradient and fractionated by two-dimensional electrophoresis using 10% polyacrylamide. Control and Ty3 VLP samples were fractionated on gels where the IEF range was pH 4 to 8 and 3.5 to 10. The latter gel was used for preparing the 38-kDa Gag3 protein for mass spectrometry because it ran at the edge of the pH 4 to 8 IEF (theoretical pI = 8.65). In the 2D gel analysis, the spot associated with p31 was diffuse compared to other species, and minor spots unique to the Ty3-containing sample flanked the CA spot. Gel slices were minced, proteins were subjected in situ to trypsin digestion, and peptides were eluted and analyzed. MALDI-MS analysis was performed on the tryptic peptides (Protein Chemistry Core Facility, HHMI/Columbia University) as described in Materials and Methods. The tryptic peptide assignments to the three major Ty3 Gag3 species are shown in Fig. 1. The predicted and observed masses upon which these assignments were based are shown in Table 1. Analysis of peptides from Gag3, CA, and p31 showed that each of these protein species has an N terminus at Ser (position 2) and that it is acetylated. The C-terminal peptide for the major CA species (fragment 11.1 in Fig. 1 and Table 1) has its carboxyl terminus at aa 207. Assuming that this is the carboxyl terminus of the protein, CA has a mass of 23,962 Da. Ty3 protein species migrating near CA were all identified by MALDI-MS analysis of tryptic peptides. The basis for the gel mobilities of these CA species was not readily determined from the tryptic peptides for each. The most C-terminal-predicted peptide for the 31-kDa protein had its carboxyl terminus at aa 191. However, there was a large, unidentified peptide at m/z = 4,901.63. If the 31-kDa protein extends to aa 233 (i.e., adjacent to the previously identified amino terminus of NC [40]), the C-terminal peptide would be aa 192 to 233 with m/z = 4,741.93 (fragment 11.2 in Fig. 1 and Table 1). This peptide is 160.58 less than the identified peptide. However, the identified peptide is consistent with a C terminus at aa 233 with two phosphorylated residues. A peptide was also detected with a mass of 4,821.91, close to the 4,821.03 predicted for the mass of the aa 192 to 233 peptide modified by phosphorylation at one site. Consistent with this prediction is the fact that the polyprotein Gag3 precursor also lacked the expected peptide from this region. For Gag3, the peptide from that region would be from aa 192 to 236, with m/z = 5,098.33 (fragment 11.3 in Fig. 1 and Table 1). Instead there is a larger peptide at 5,258.91, also a 160.58 difference. If this region contains two phosphorylated residues, then the intermediate previously referred to as p31 would have an unmodified mass of

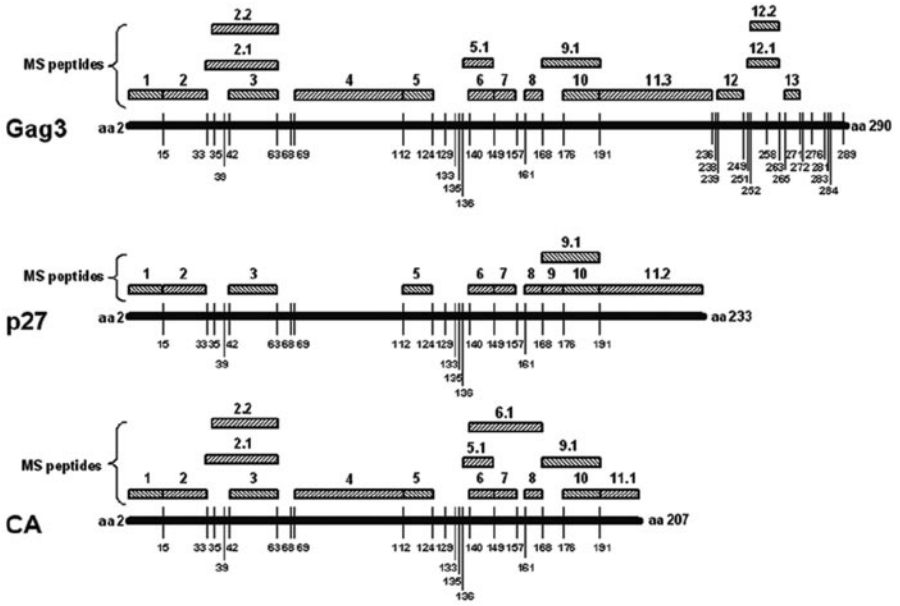

FIG. 1. Coverage of Gag3, p27, and CA by tryptic peptides. The presumptive primary protein structures for Gag3, p27, and CA are depicted as heavy black lines beginning on the left at amino acid 2 (aa 2). Numbering of amino acids is according to the theoretical Gag3 ORF beginning with the first Met codon. The positions of trypsin cleavage sites (arginine residues) are shown throughout each protein as slashes, with the numbers below indicating the aa positions of the arginine residues. Actual tryptic peptides matched to Gag3, p27, and CA are shown above each protein as hatched boxes (MS peptides). Mass data for the tryptic peptides are shown in Table 1.

26,989 Da and the cleavage that creates the amino terminus of NC would also create the carboxyl terminus of this protein. As this is the simplest interpretation of the data, the protein previously referred to as p31 will be referred to as p27 and Gag3/p38 will be designated Gag3/p34. If p27, ending at the amino terminus of NC, is processed once by a cleavage between residues 207 and 208 to generate CA, a spacer peptide containing residues encoded from codons 208 to 233 of *GAG3* would also be generated. This hypothetical peptide would have a mass of 3,045 Da and is designated p3. Immunoblot analysis of Ty3 VLP proteins using anti-phosphotyrosine, anti-phosphoserine, and anti-phosphothreonine indicated that Gag3 is phosphorylated on multiple residues, but because CA also showed this reactivity, it was not possible to infer the phosphorylation pattern of the p3 region specifically (data not shown).

The cleavages demonstrated and inferred from this analysis are shown in Fig. 2A. Ty3 PR is an aspartyl protease homologous to retroviral proteases. Cleavage sites of retroviral proteases are not highly conserved but are determined primarily by local context, including residues P4 to P3′ with hydrophobic residues overrepresented at positions P1 and P1′ (70). In previously observed Ty3 cleavage sites, hydrophobic residues were overrepresented at P3 (3 out of 5), P2 (4 out of 5), and P2′ (5 out of 5) but not P1 and P1′ (40). In the case of the Ty3 CA-P3 cleavage site newly described here, hydrophobic residues occupy positions P3 (I) and P2 (I) but not P2′ (T) (Fig. 2B).

Ty3 VLPs are heterogeneous in size and ordered. Ty3 was expressed and VLPs were isolated and characterized by AFM. The AGY-9 strain was chosen for expression of Ty3 for VLP characterization, because AGY-9 has been demonstrated to produce Ty1 and Ty3 particles efficiently with the Ty element under control of the *GAL1-10* upstream activating sequence (25 and unpublished data). Under these conditions, it was anticipated that the major source of particles in the cell would be Ty3 (28). Although Ty1 mRNA constitutes a significant percentage of total RNA in typical wt strains (17), Ty1 protein is unstable and so Ty1 protein and particles are not readily detectable in the absence of Ty1 overexpression (16). In addition, the AGY-9 strain contains a mutation in *spt3* so that the full-length, 5.7-kb Ty1 RNA is not produced (85). Ty1 *TYA*-encoded protein was undetectable and judged to be less than 0.01 μg per 0.5 μg of VLP preparation by immunoblot analysis of this fraction (data not shown).

In order to regulate production of Ty3, AGY-9 cells were transformed with pDLC201, a high-copy plasmid marked with *URA3*, from which Ty3 is expressed under the *GAL1-10* upstream activating sequence, or with the related vector pYES2.0 (Invitrogen Inc., Carlsbad, CA). Transformants were isolated on SD-ura and grown to log phase in SR-ura. Ty3 expression was induced with the addition of galactose to 2%, and cells were grown for an additional 24 h. A fraction enriched for Ty3 VLPs was prepared by separating whole cell extracts over a 20/30/70% sucrose gradient as described in Materials and Methods. One-hundred seventy-five-microliter aliquots of the 30/70% interface from the control and the Ty3-expressing cultures were examined directly for Ty3 proteins and particles.

Aliquots of protein from the interface of sucrose gradients in which control and Ty3-expressing cell extracts were fractionated were analyzed by denaturing polyacrylamide gel electrophoresis. Coomassie-stained gels of these preparations showed that Ty3 Gag3 and CA were major components of the VLP-enriched fraction from cells expressing Ty3 (data not shown). Immunoblot analysis using anti-CA showed Gag3/p34, p27, and CA/p24 species in fractions from cells expressing wt Ty3 (Fig. 3, lanes 1 and 5) but did not show detectable Ty3 species in the control preparations (Fig. 3, lanes 4 and 8).

TABLE 1. Peptides identified by mass spectrometry and assigned to p27, CA, and Gag3

Peptide[a]	Position[b]	#MC[c] no.	Modification[d]	Calculated mass[e]	p27 mass[f]	p27 ΔDa[g]	CA mass[h]	CA ΔDa[i]	Gag3 mass[j]	Gag3 ΔDa[k]
1	1–15	0		1642.88						
1	1–15	0	−Met +acetyl	1553.88	1553.71	0.17	1553.93	−0.05	1553.92	−0.04
1	1–15	0	−Met +acetyl, MetOx (XI)	1569.87	1569.72	0.15	1569.89	−0.02	1569.92	−0.05
2	16–33	0		2072.47	2072.18	0.29	2072.27	0.2		
2	16–33	0	Cys PAM	2143.55	2143.32	0.23	2143.89	−0.34	2143.84	−0.29
2.1	34–63	3		3494			3493.83	0.17	3493.68	0.32
2.2	36–63	2		3280.76			3280.58	0.18	3280.12	0.64
3	43–63	0		2457.84	2457.65	0.19	2457.96	−0.12	2458.1	−0.26
3	43–63	0	MetOx (X1)	2473.83	2473.65	0.18	2473.94	−0.11	2474.09	−0.26
3	43–63	0	MetOx (X2)	2489.82	2489.52	0.3	2490.02	−0.2	2490.22	−0.4
3	43–63	0	MetOx (X3)	2505.81	2505.44	0.37	2506.03	−0.22	2506.03	−0.22
3	43–63	0	MetOx (X4)	2521.8	2522.18	−0.38				
4	70–112	0		5062.7			5062.38	0.32	5062.65	0.05
5	113–124	0		1335.54	1335.75	−0.21	1335.92	−0.38	1335.84	−0.3
5.1	137–149	1		1666.95			1667.13	−0.18	1666.89	0.06
5.1	137–149	1	MetOx (X1)	1682.94			1683.39	−0.45	1683.24	−0.3
5.1	137–149	1	MetOx (X2)	1698.93			1698.83	0.1	1698.51	0.42
6	141–149	0		1096.3	1096.52	−0.22	1096.59	−0.29	1096.68	−0.38
6	141–149	0	MetOx (X1)	1112.29	1111.95	0.34	1113.06	−0.77	1112.41	−0.12
6.1	141–168	3		3335.96			3335.87	0.09		
7	150–157	0		927.11	927.31	−0.2	927.61	−0.5	927.21	−0.1
8	162–168	0		895	895.29	−0.29	895.44	−0.44	895.07	−0.07
9	169–176	0		984.2	984.83	−0.63				
9.1	169–191	1		2695.03	2695.93	−0.9	2695.88	−0.85	2696.21	−1.18
10	177–191	0		1729.87	1729.72	0.15	1730.08	−0.21	1729.98	−0.11
10	177–191	0	MetOx (X1)	1745.86	1745.7	0.16	1746.04	−0.18	1746.11	−0.25
11.1	192–207	0		1714.86			1715.26	−0.4		
11.2	192–233	0	2 PHOS	4901.89	4901.63	0.26				
11.2	192–233	0	1 PHOS	4821.91	4821.03	0.88				
11.2	192–233	0	no PHOS	4741.93						
11.3	192–236	0	2 PHOS	5258.29					5258.91	−0.62
11.3	192–236	0	1 PHOS	5178.31						
11.3	192–236	0	no PHOS	5098.33						
12	240–249	0		1234.38					1234.52	−0.14
12.1	252–263	2	Cys PAM	1531.7					1531.93	−0.23
12.2	253–263	1	Cys PAM	1375.51					1375.8	−0.29
13	266–271	0	Cys PAM	919.14					919.41	−0.27

[a] Peptides corresponding to MS peptides numbered in Fig. 1 showing coverage of Gag3, p27, and CA by mass spectrometry data.
[b] Position indicates peptide end points within the Gag3 ORF.
[c] #MC indicates the number of missed cleavages by trypsin during digestion prior to mass spectrometry.
[d] Modifications indicate posttranslational modifications in vivo or sample processing changes in vitro that affect peptide mass: −Met +acetyl is removal of initiator methionine and acetylation of N-terminal serine; Cys PAM is propionamide cysteine; MetOx is oxidized methionine (number indicated); PHOS is phosphorylations (number indicated).
[e] Calculated masses (*m*/*z*) of peptides generated by tryptic digestion of Gag3 and derivatives. Masses were generated by a theoretical tryptic digestion using the Peptide Mass program on the ExPaSy website (http://au.expasy.org//tools/peptide-mass.html) using average masses of the amino acid residues and giving peptide masses as $[M + H]^+$.
[f] Peptide masses (*m*/*z*) from tryptic digestion of Ty3 p27 that can be assigned to p27.
[g] Differences (in Daltons) between the masses of peptides assigned to p27 and the calculated masses of the corresponding peptides generated by theoretical tryptic digestion.
[h] Peptide masses (*m*/*z*) from tryptic digestion of Ty3 CA protein that can be assigned to CA.
[i] Differences (in Daltons) between the masses of peptides assigned to CA and the calculated masses of the corresponding peptides generated by theoretical tryptic digestion.
[j] Peptide masses (*m*/*z*) from tryptic digestion of Ty3 Gag3 protein that can be assigned to Gag3.
[k] Differences (in Daltons) between the masses of peptides assigned to Gag3 and the calculated masses of the corresponding peptides generated by theoretical tryptic digestion.

The sucrose gradient interface preparations from control and Ty3-expressing cells were spread directly on lysine-coated slides, subjected to gentle fixation, and imaged by AFM under buffer at physiological pH as described in Materials and Methods. The diameter of particles was determined by measuring the height of particles relative to substrate. In the case of the control cell extracts from AGY-9 cells not expressing Ty3, particles were observed ranging from 22 to 39 nm in diameter with a mode of 35 nm. These particles appeared to have a relatively smooth surface, and no ordered structure was apparent (Fig. 4A and B).

In extracts from cells expressing wt Ty3 (Fig. 4C and D), particles were much more concentrated than in cells not expressing Ty3 and differed dramatically in appearance (Fig. 4, compare A and B with C and D). In contrast to the particles observed in control cell extracts, these particles displayed regular patterns of capsomeres on their surfaces (12, 32, 73). These structured particles, which were only observed under conditions of Ty3 expression and which were concentrated in the interface fraction enriched for Ty3 protein, were concluded to be Ty3 VLPs.

Measurement of several preparations of VLPs from cells expressing wt Ty3 showed well-ordered particles of a range of sizes. Figure 5 is a histogram of the diameters of 150 ordered wt particles based on heights above background. These particles ranged in size from about 25 nm to 52 nm in diameter.

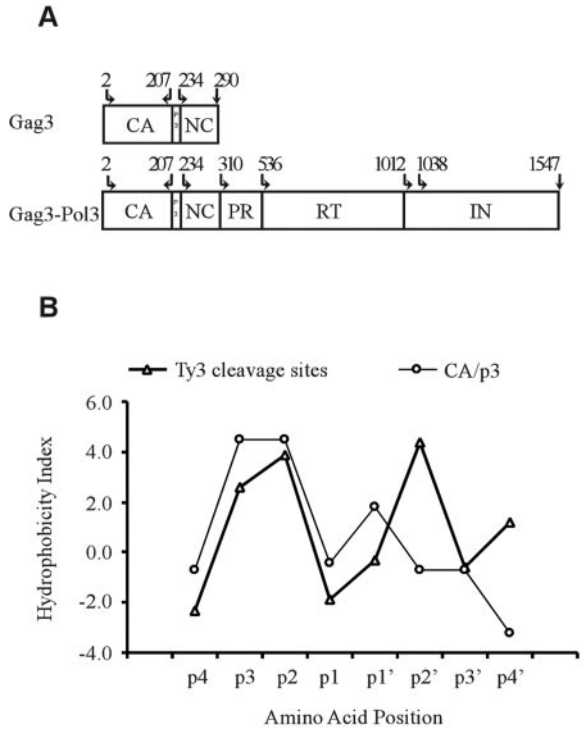

FIG. 2. Ty3 Gag3 processing. (A) Diagram indicating inferred processing sites for Ty3 Gag3 and Gag3-Pol3. Open boxes indicate Ty3 polyprotein precursors Gag3 and Gag3-Pol3. Amino-terminal processing of Gag3 and Gag3-Pol3 and processing to create p34 (aa 2 to 290), p27 (aa 2 to 233), and CA p24 (aa 2 to 207) were as determined in this study. Amino termini of PR, RT, and IN were determined previously (40). (B) Hydrophobicity plot of Ty3 cleavage sites P4 (amino terminal) to P4′ (carboxyl terminal) flanking the scissile bond. Five previously described Ty3 PR cleavage sites were assigned hydrophobicity scores at positions P4 and P4′ according to Kyte and Doolittle (46). These scores were averaged and plotted (triangles). The average is compared to the hydrophobicity of residues flanking the newly described CA-P3 site (circles).

Other wt preparations varied in distribution over a similar range but were also heterogeneous in diameter (data not shown).

The surfaces of ordered particles exhibited regular arrangements of capsomeres. Although capsomeres were prominent, they did not extend far above the VLP surface, and we would hesitate to call them "spikes." A clear substructure to the capsomeres that would imply resolution of single capsid proteins could not be discerned. However, a pentameric capsomere could be discriminated from a hexameric capsomere by its environment (Fig. 6), as capsomeres were points of local fivefold or sixfold rotational symmetry. The capsomeres were separated by pronounced surface depressions. The AFM tip, because of its finite radius of curvature, cannot penetrate deeply into depressions. Thus, the depressions are likely to be greater than they appear in the images and may represent actual holes in the VLP surfaces. The depressions are 3 to 4 nm in extent. In almost all of the images, the substrate is cluttered with small objects of more or less uniform size. Although appearing of greater lateral extent, their heights are no more than a few nanometers. These could be pentameric or hexameric aggregates of the capsid protein.

A minor fraction of particles in the AFM images of wt Ty3 particles did not exhibit structure, similar to what was observed in cells not expressing Ty3. These unstructured particles ranged in size from 27 to 36 nm. This fraction was variable among experiments but was always less than 10% of total particles. We concluded that many of the unstructured particles we observed were not related to Ty3. However, we could not formally exclude the possibility that a subset of them are.

Because Ty3 expression was ongoing in this culture, it was anticipated that VLPs would represent different stages in particle morphogenesis. Under these conditions, transposition and cDNA can be readily measured within 6 h (57). The interpretation that the Ty3 VLPs were likely to be at different stages of morphogenesis was also supported by the presence of Gag3 as well as processed species (Fig. 3).

Ty3 PR activity is not required for ordered Ty3 particle structure. Activation of retroviral PR by dimerization appears to be dependent on assembly (11), and subsequent proteolytic processing and remodeling into distinctive core structures occurs concurrent with budding from the host cell surface. In order to determine whether Ty3 PR processing of the Ty3 VLP Gag3 and Gag3-Pol3 is accompanied by structural rearrangement of the VLP, we simulated the immature Ty3 core using Ty3 mutated in the catalytic site of the Ty3 PR (D59I) (40) and the mature core using Ty3 mutated in a conserved residue of RT (D213N).

AGY-9 was transformed with pJK776, which carries the Ty3 PR mutant, and transformants were isolated and grown under inducing conditions for Ty3 expression. The Ty3 VLP fraction from cells expressing the PR mutant was examined by immunoblot analysis using anti-CA and anti-IN (Fig. 3, lane 6). This analysis confirmed, as previously reported (40), that the PR mutant accumulates Ty3 Gag3 and Gag3-Pol3 precursor polyproteins. Inspection of the immunoblot pattern produced with anti-CA showed Gag3 and a minor amount of species which

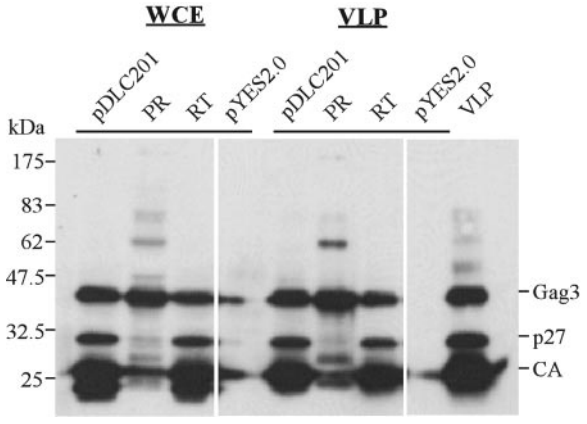

FIG. 3. Immunoblot analysis of Ty3 VLP preparations. Whole-cell extracts of cells expressing wt Ty3 (pDLC201) and PR (pJK776) and RT (pTy3RTD213N) mutant Ty3 elements and vector alone (pYES2.0) (left panel, 5 μg protein per lane), and Ty3 VLPs prepared from sucrose step gradients from the same whole-cell extract (WCE) (right panel, 0.2 μg protein per lane) were fractionated on a SDS–10% polyacrylamide gel. Proteins were transferred to Immobilon membrane and reacted with anti-CA and secondary antibody as described in Materials and Methods.

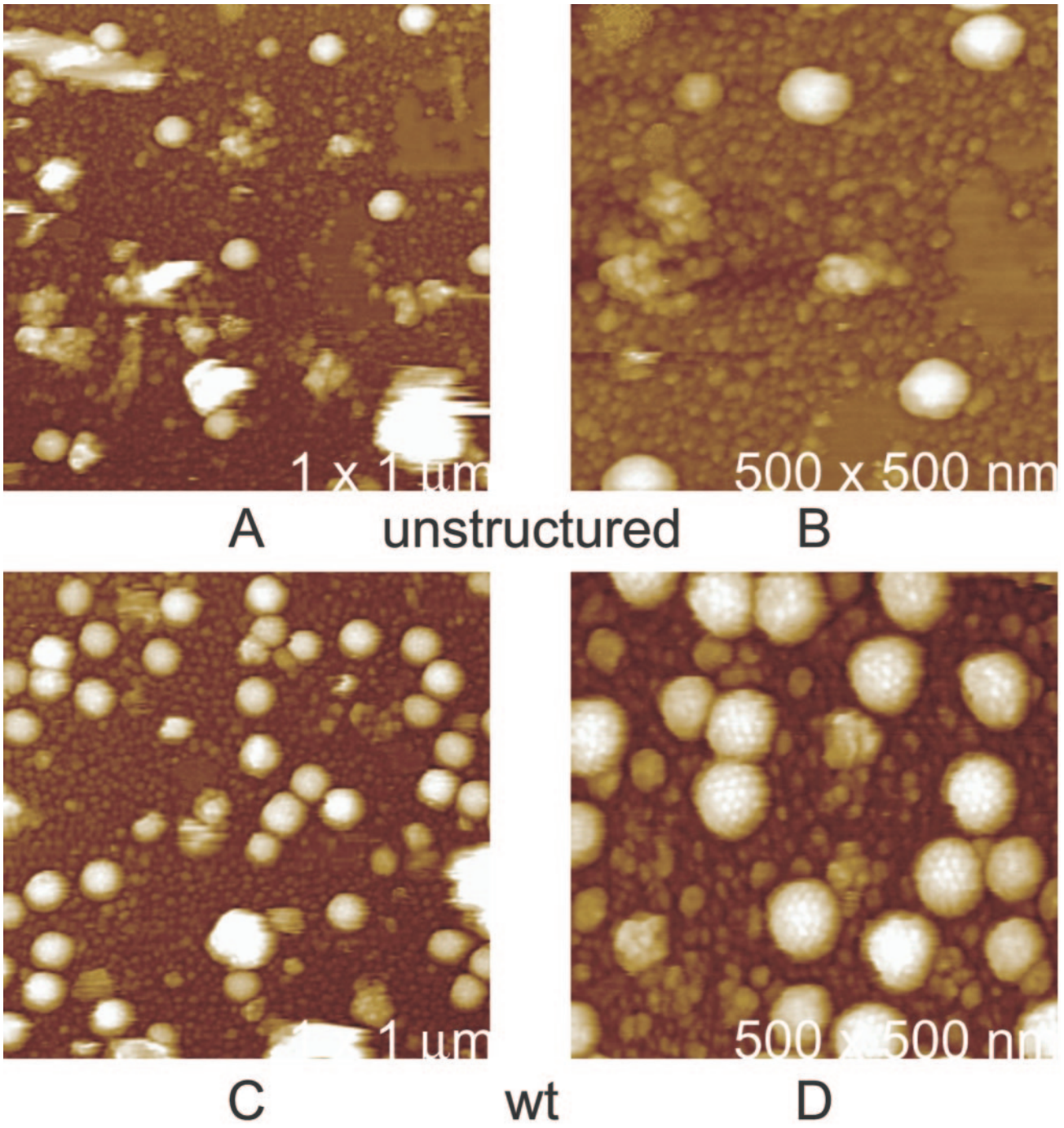

FIG. 4. Ty3 wt VLPs imaged by AFM. VLP fractions were prepared from cells grown under inducing conditions, and aliquots of the enriched sucrose step gradient 30/70% interface fractions were fixed and imaged directly as described in Materials and Methods. Dimension of scan is indicated at lower right of each panel. Panels A and B, extracts from cells transformed with vector only; panels C and D, extracts from cells induced to express wt Ty3 from pDLC201.

reacted with anti-CA but which were for the most part not observed in preparations from cells expressing wt Ty3 (Fig. 3, lanes 5 and 6). These minor species are similar in size or smaller than CA and presumably represent proteolytic breakdown products of Gag3. Formally, Gag3 cleaving activity could be attributable to leaky Ty3 mutant activity. However, based on the catalytic mechanism of aspartyl proteases such as Ty3 PR, it would be surprising if the D59I mutation at the catalytic site allowed residual activity. As mentioned above, AGY-9 has endogenous Ty3 elements and so formally proteolysis could be attributed to endogenous elements. However, as indicated previously, expression of these elements is not detectable. In addition, the Ty3 PR mutant was expressed in yTM443 (4), from which endogenous Ty3 elements have been deleted and a similar anti-CA immunoblot pattern was observed (data not shown). Collectively these data argued that the Ty3 PR mutant is

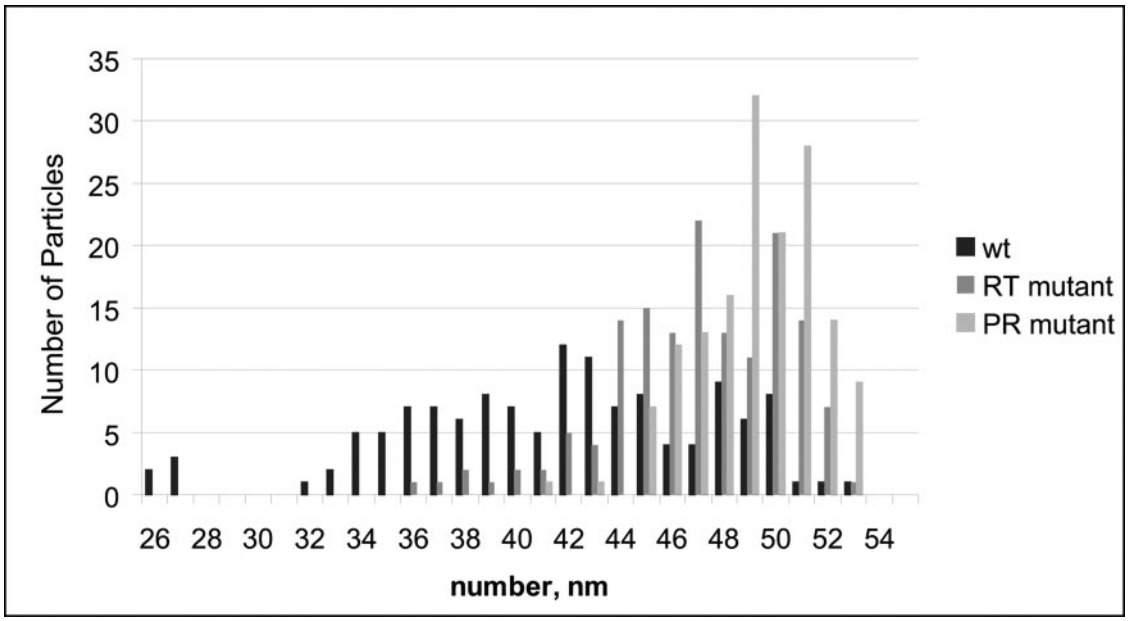

FIG. 5. Histogram of height of ordered Ty3 wt and PR and RT mutant VLPs. VLP fractions were prepared from cells expressing wt Ty3 as well as cells expressing either the PR or RT mutant of Ty3. For wt, 150 particle diameters were measured according to particle heights above background; for PR mutants, 154 particles; and for RT mutants, 149 particles.

blocked for Ty3 processing. Thus, the Gag3-related species of lower molecular weight are most likely created by non-Ty3 PR activities.

The majority of particles from the PR mutant were from 44 to 53 nm in diameter. The average diameter for 154 ordered particles was 49 nm ± 2.3 nm. In other respects, the PR mutant particles were very similar in morphology to the wt Ty3 (Fig. 7A and B compared to C and D).

Ty3 RT mutants form ordered VLPs. Proteolytic processing is required for production of mature RT, but for most retroviruses reverse transcription occurs primarily in the host cell rather than the virion. In order to model the VLP at a stage analogous to that of the characteristic viral core in the mature virion, Ty3 mutated in residues essential for RT catalytic activity (D213N) was used. The D213N mutation was shown to cause loss of recombinant protein RNaseH activity and RNA-templated DNA polymerase activity in vitro and, in the context of the full-length Ty3, loss of transposition activity in vivo (71 and D. Lener and S. LeGrice, National Cancer Institute, Frederick, MD, personal communication).

VLPs were prepared from cells expressing the RT D213N mutant Ty3 in order to examine mature VLP morphology. The VLP fraction was subjected to denaturing gel electrophoresis and immunoblot analysis. This analysis showed that, as expected, the pattern of RT mutant Ty3 Gag3 and CA processing products was indistinguishable from that of the wt Ty3 proteins (Fig. 3, lanes 1 and 5 compared with lanes 3 and 7). However, examination of the VLP fraction by AFM showed that, like the PR mutant, only larger sized, ordered particles were observed. The majority were 44 to 52 nm in diameter for a set of 149 particles with an average ordered particle diameter of 48 nm ± 2.3 nm. The external appearance of the RT mutant VLPs was essentially indistinguishable from that of the wt and PR mutant VLPs (Fig. 7A and B compared to E and F).

Ty3 particles exhibit distributions of capsomeres on their surfaces consistent with icosahedral symmetry. Caspar and Klug (12) postulated that spherical viruses could be constructed according to icosahedral symmetry and that discrete classes of particles so formed could be described by integral T numbers which defined the number and distribution of protein subunits and capsomeres on their surfaces. Capsomeres are of two types, those composed of five protein subunits and having fivefold symmetry, of which there are always 12, and a variable number of capsomeres composed of six protein subunits exhibiting threefold (pseudo-sixfold) symmetry. Subsequent analyses by X-ray diffraction and electron microscopy have, for the most part, confirmed their theory, though exceptions have been found.

Among the exceptions are polyomavirus, composed only of pentamers (72), and various capsids which, though not strictly icosahedral, are derived from icosahedral principles, such as alfalfa mosaic virus (33). An exception which deserves particular note, however, is the capsid of HIV, which is generally conical in shape and is likely formed of fivefold and sixfold capsomeres that are distributed in a pattern consistent with fullerene cone principles rather than rigorous icosahedral symmetry (24). Furthermore, no one has yet succeeded in demonstrating that the capsid of another retrovirus, MLV, is strictly icosahedral. Indeed, evidence exists that it too may deviate from strict icosahedral symmetry (86).

Thus, we feel it wise to be somewhat circumspect in the interpretation of our AFM images of the Ty3 VLPs, because they are closely related, perhaps homologous to retroviral capsids. This is especially so because we can, with AFM, visualize only the exposed surface areas of sample particles. In addition, there is particle distortion due to tip radius, tip pressure, and the deformability of the particles themselves.

Nevertheless, the AFM images of Ty3 VLPs show them to

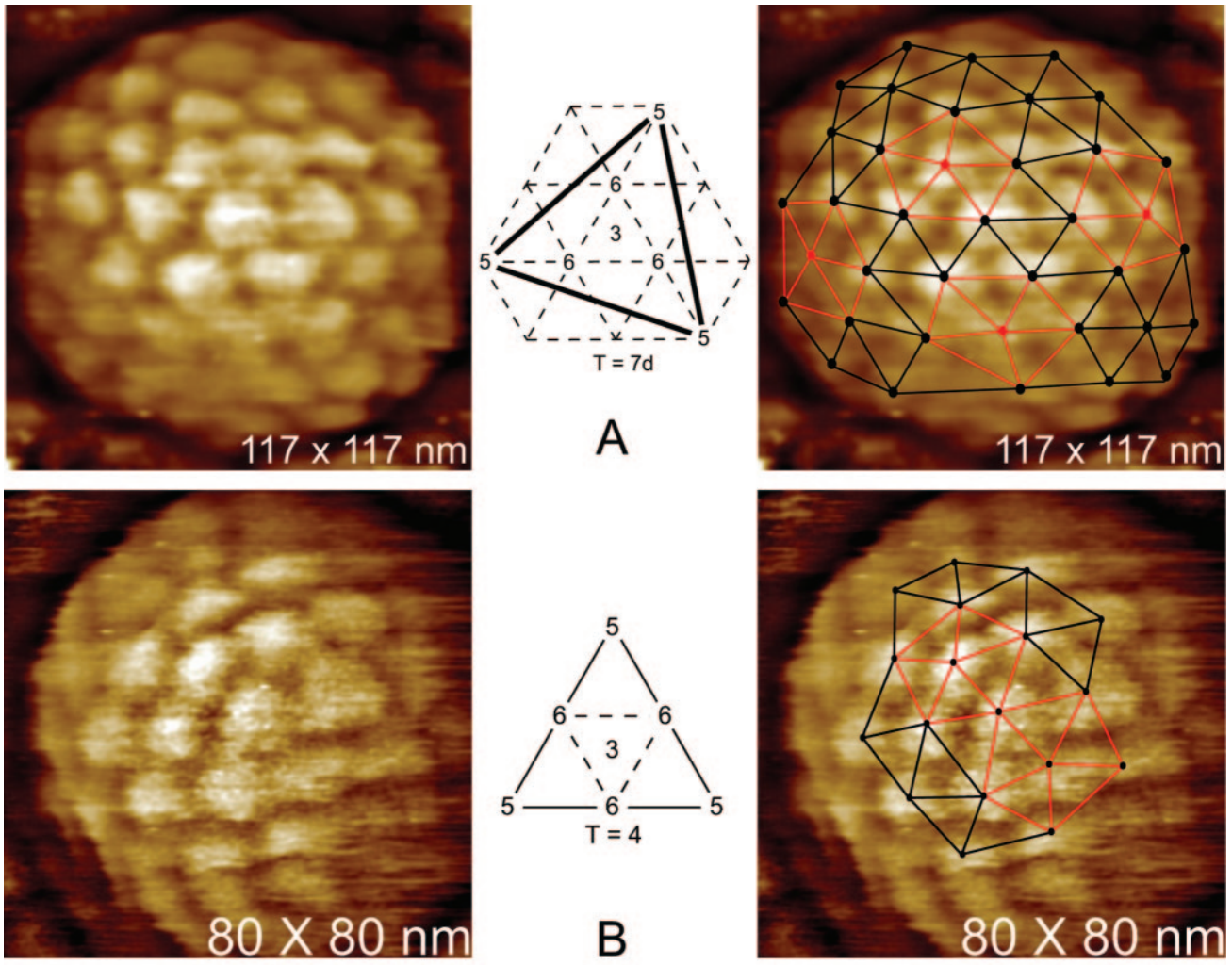

FIG. 6. Icosahedral structure of wt Ty3 VLP imaged by AFM. (A) Left and right panels, wt Ty3 particle. Scale of scan is shown. Right panel, hexagonal net overlay corresponding to T=7 showing pentagonal vertices in red. Center, diagram of triangular face of icosahedron showing positions of pentagonal and hexagonal capsomeres for T=7. (B) As described above for panel A, but illustrating the relationship of pentons in a T=4 arrangement of capsomeres. Because the entire particle is not imaged, these relationships illustrate local features of particles rather than proving them to be T=7 and T=4.

be spherical on average and to exhibit distributions of capsomeres on their surfaces consistent with icosahedral symmetry. No particles were observed that definitively failed icosahedral constraints, but we cannot exclude the possibility that particles are a mixture of forms, including some which lack icosahedral symmetry. Inspection of hundreds of wild-type VLPs showed that they could be sorted into three classes, and that these ranged in sizes consistent with T=7, 4, and 3 icosahedra.

The determination of T number within each class was made by two methods, first based on the lengths of the edges of the equilateral triangular facets defined by three neighboring capsomeres and the second based on the distribution of pentameric and hexameric capsomeres on a VLP surface.

The surface area of a PR mutant particle (average diameter, 49 nm) is 7,539 nm^2. Measurement of the distance from capsomere center to capsomere center provides the length of the edge of a triangular facet. Eighty measurements were made on seven PR mutant particles, yielding an average length of 11.35 nm (± 0.9 nm). If a T number of 7 is assumed, then the capsomere center-to-center distance is calculated to be 11.15 nm, which is well within the experimental error. The T number can also be obtained directly by counting the number of hexameric capsomeres lying between pentameric capsomeres. Using the latter approach, an example of a net consistent with T=7 is shown in Fig. 6A.

Measurement of the capsomere center-to-center distance for eight wt particles presumed to be of T=4 icosahedral symmetry yielded a value of 10.7 nm (± 1.3 nm). This is, within

FIG. 7. PR and RT mutant Ty3 VLPs imaged by AFM. Aliquots of the VLP-enriched fraction of sucrose step gradient interface fractions of cells expressing the Ty3 PR and RT mutants were prepared and imaged as described for wt Ty3 VLPs in the legend of Fig. 4. A and B, Ty3 wt VLPs; C and D, Ty3 PR mutant VLPs; and E and F, Ty3 RT mutant VLPs. Dimension of scan is indicated at lower right of each panel.

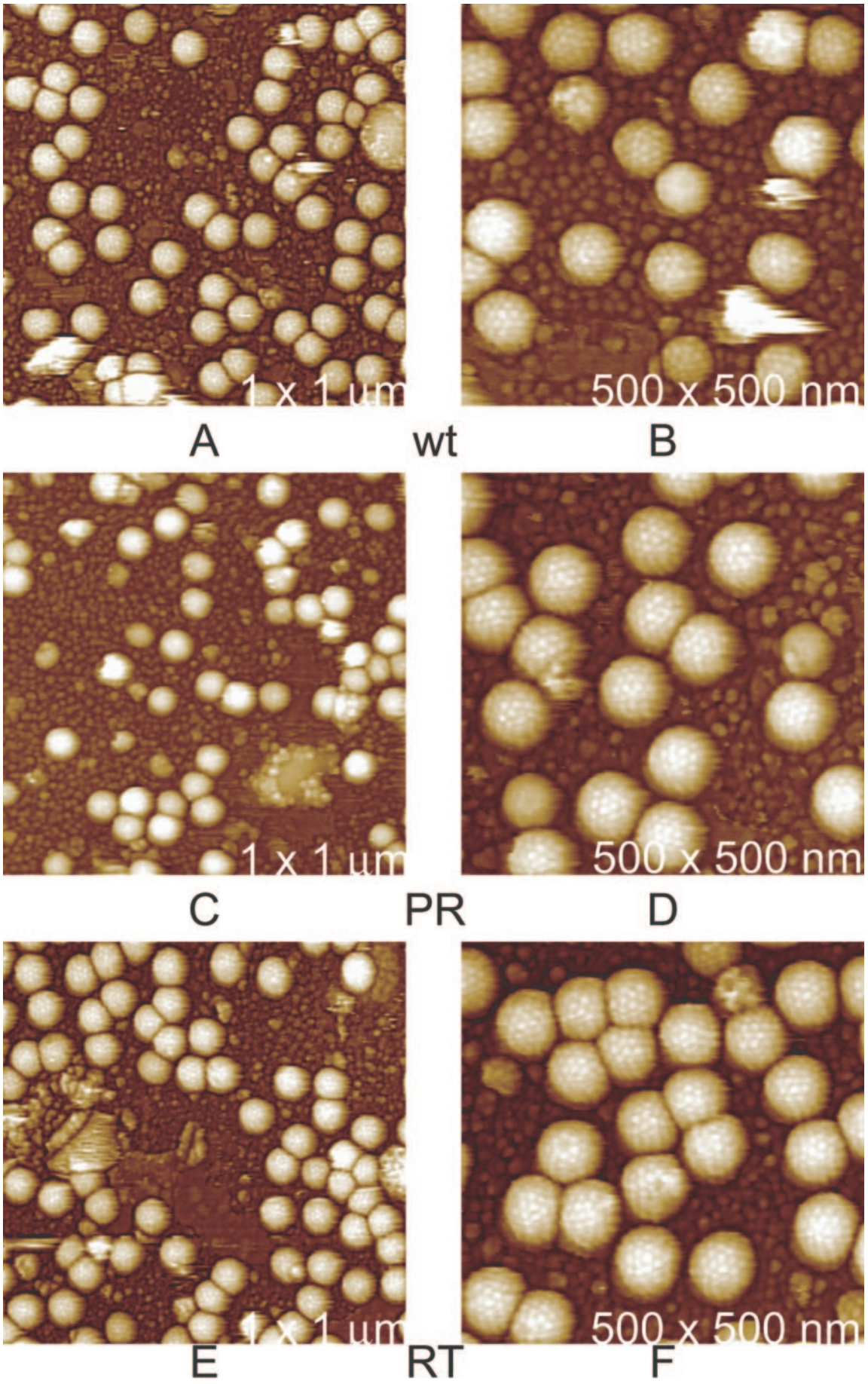
1 x 1 um
500 x 500 nm
A
wt
B
1 x 1 um
500 x 500 nm
C
PR
D
1 x 1 um
500 x 500 nm
E
RT
F

experimental error, virtually the same as for the larger particle, consistent with assumption of discrete icosahedral T numbers. VLPs with a diameter of 37 nm have a surface area of 4,308 nm^2. From this, the edge length, assuming T=4, is 11.15 nm, which is, again, well within experimental error of the measured edge length. A net consistent with T=4 icosahedral symmetry is indicated in Fig. 6B. Because of the small radius of curvature of the particle face, it was not possible to align a hypothetical net with the surfaces of the smallest particles which were concluded to be T=3.

T=7 icosahedra are noncentrosymmetric and can exist in two enantiomorphs, designated d and l. Because height information is retained in AFM, we can discriminate the two. The grid, and hence the particle lattice, corresponds to the d enantiomer, and the larger class of particles would, therefore, be icosahedra of T=7d.

DISCUSSION

The Ty3 element encodes the major structural polyprotein Gag3, which is required for successful completion of the life cycle. In this study, the products of Gag3 processing and the morphological transition from immature to mature Ty3 VLP were further defined. The Ty3 VLP has interesting parallels and differences with retrovirus core particles. The immature Ty3 particle is assembled from Gag3 and Gag3-Pol3 into roughly spherical particles functionally analogous to immature retrovirus core particles. During maturation, Ty3 Gag3 is processed into CA, p27, NC, and possibly a p3 species, similar to what occurs for retrovirus Gag. However, for Ty3, this transition occurs within the cytoplasm, while for most retrovirus virions it occurs concomitant with budding from the cell. We found that this transition further differs molecularly, because Ty3 proteolytic processing is not accompanied by the dramatic remodeling that accompanies retrovirus core particle maturation. For many retroviruses this includes development of a heterodisperse core particle morphology (13) and, at least for some viruses, loss of a large fraction of CA from the core itself (7), whereas for Ty3 the mature form is externally similar to the immature form. Finally, the product of Ty3 proteolytic maturation appears to be relatively stable compared to most mature retrovirus cores stripped of virion membrane. For example, Ty3 VLPs were resistant to stresses such as conditions of centrifugation (28 and unpublished data) that can dissociate a significant percentage of retrovirus cores from which membranes have been removed (13, 20).

Ty3 Gag3 maturation. After Ty3 VLP assembly, the major structural polyprotein precursor, Gag3 (aa 1 to 290), is processed by Ty3 PR into the components of the mature particle. In our study we showed that Gag3 and its derivatives have the amino-terminal Met removed so that Ser at aa position 2 becomes the amino-terminal residue. Ser was modified by acetylation in Gag3, p27, and CA. The Gag3-derived p27 beginning at aa 2 was inferred to have its carboxyl terminus at aa 233. CA/p24 extends from aa 2 to 207. NC was previously shown to have its amino terminus at aa 234. A p3 spacer (aa 208 to 233) was inferred to occur flanked by CA and NC domains.

Comparison of the 289-aa CA-p3-NC domain of the amino-terminally processed Ty3 Gag3 to retrovirus Gag CA-spacer-NC domains shows that it is comparable in length and function. For example, HIV-1 CA is 231 aa in length, the encoded spacer is 14 aa, and NC is 55 aa, for a total length of 300 aa (13). Mutations in the Ty3 CA MHR motif (65), similar to mutations in the retrovirus MHR (15), cause pleiotropic phenotypes, including disruption of particle formation, processing, DNA synthesis, and transposition. In the case of HIV and RSV, a spacer peptide between CA and NC must be processed to complete particle assembly (15, 69). Cleavage between the CA domain and spacer is one of the last Gag cleavages in retrovirus core maturation (78), and specific chemical inhibitors of this step have been isolated, indicating that the cleavage site may have distinct substrate features (89). It is interesting that in the case of Ty3, this site lacked the hydrophobic residue found at position P2′ of other Ty3 PR cleavage sites, suggesting that its processing could be temporally differentiated from those of other sites. Although the p3 spacer is not essential for Ty3 transposition, deletion mutants in this region differ in transposition frequency (M. S. Aye and S. B. Sandmeyer, unpublished data), suggesting that it could perform a regulatory function. Consistent with that possibility, mass spectrometry suggested that this domain is phosphorylated in Gag3 and p27. Ty3 NC has one copy of the zinc finger domain, and mutations in conserved His and Cys residues cause disruption of particle morphogenesis (66). Thus, Ty3 CA-p3-NC is not only comparable in length but also in function to a subdomain of retroviral Gag.

MA-CA-NC domains of Gag have been localized in immature particles by cEM for RSV (88), HIV (84), and MLV (86). These studies indicate that the Gag precursor is radially arrayed, with the amino termini on the outside of the immature spherical particle and a relatively disordered NC domain proximal to the interior. A similar configuration of Ty3 would mean that the capsomeres observed by AFM are composed of CA. The fact that Ty3 Gag3 does not include an MA-like domain has several implications for Ty3 morphogenesis compared to that of retroviruses. Retroviruses, including MLV and HIV-1, which assemble on the plasma membrane, do so in part because myristylated MA targets Gag to the plasma membrane (13, 76). Ty3 assembly is not observed in association with the plasma membrane (unpublished data), and consistent with that, acetylation of Gag3 would not a priori be expected to target Gag3 to the plasma membrane. In the case of HIV-1 and RSV, it has been shown that proteolytic cleavage between MA and CA during maturation creates an amino terminus of CA, which then interacts with an internal acidic residue to stabilize a new, mature CA-specific structure (22, 26, 59, 80). Ty3 Gag3, in contrast to retrovirus Gag, would be processed at its amino terminus only by removal of the initiator Met and acetylation and thus would not be anticipated to undergo the rearrangement observed after proteolysis for retrovirus CA domains. This would explain the external similarity between the immature Ty3 PR mutant VLPs and mature RT mutant VLPs.

Ty3 particles are bounded by open icosahedral nets of capsomeres. Within the limits of the AFM technique, the images indicate that Ty3 VLPs exhibit surface distributions of pentameric and hexameric capsomeres consistent with T=7 and 4 icosahedral symmetry. The icosahedral organization is supported as well by the consistency of the capsomere-to-capsomere distance for all particles, which indicates that the different size classes differ only by the number of triangular facets and not

their size. Additionally, icosahedral nets of T=7 and T=4 symmetry were directly superimposable on visible portions of several VLPs. We cannot rule out that particles may be present which deviate from strict icosahedral symmetry, but we could identify none with certainty. Apparent violation of strict icosahedral symmetry by some closely related retroviruses, however, deserves consideration and suggests caution.

The broad, continuous distribution of wt particle sizes can be reconciled with the icosahedral classes described above if it is assumed that the diameters of particles within a class can vary over a range of 10 to 15%. This is not unrealistic, given the tenuous, open network of protein capsomeres that comprise the capsids of the VLPs. In addition, there are numerous examples of virus capsids composed only of protein that swell or contract over such a range. This may occur as a function of pH, salt concentration, preparative procedure, or physiological state (36). In addition, wt particles investigated here represent all of those stages which appear throughout the Ty3 replication cycle.

Deep depressions, possibly holes, were observed between the capsomeres. The depressions make connections between capsomeres appear relatively tenuous, suggesting that the Ty3 VLP surface is a cagelike latticework rather than a dense shell. Retroviral and Ty1 particles also appear to be porous (74, 82). If the depressions are holes, the diameter of these would be great enough for entry of some types of RNase. This would explain the observed sensitivity of the wt Ty3 genomic RNA to this enzyme (data not shown). A proportion of the particles are not perfectly shaped but appear to be flattened on one or more sides. Such shapes are also observed by transmission EM of whole cells (unpublished data). This could reflect the flexibility of a porous cagelike VLP structure. Some of what we observed could be the results of compression of a flexible structure during preparation or by the AFM tip. We did not see evidence in our images of spikes or trimer clustering of subunits nor of triangular shape to the quasi-equivalent hexagonal capsomeres, as was suggested for Ty1 capsomeres (67). In comparison to capsomeres we have examined on some other viruses (44, 52), the Ty3 capsomeres are relatively blunt or even flat.

wt, but not PR or RT mutant VLPs, contain particles consistent with T=4 and like even T=3 icosahedral symmetry. We considered three explanations for the smaller ordered Ty3 particles in the wt VLP preparations. First, different diameters could be a result of stochastic processes associated with assembly, for example, particles which assemble before incorporation of nucleic acid. Second, Ty3 particles of different diameters could be composed of different amounts of Gag3-related degradation species. Third, particles of smaller diameters could represent particles at post-reverse transcription stages of morphogenesis.

The first two possibilities are that particles in different size classes assemble as a function of the kinetics of the assembly process or that the smaller diameter particles represented in the population are produced from truncated Ty3 Gag3. Observations in the case of Ty1 are relevant to these possibilities. The icosahedral particles that we observed for wt Ty3 VLPs are similar to the icosahedral particles reported for the truncated Ty1 capsid protein. Ty1 encodes its 440-aa p1 capsid protein in the *TYA* reading frame. Ty1 p1 lacks MHR and zinc finger motifs found in Ty3. However, similar to Ty3, Ty1 undergoes intracellular retrotransposition and does not have an extracellular enveloped stage or MA-like domain. Ty1 p1 is processed by Ty1 PR to form a mature p2 described as 402 or 407 aa (53, 58). Although native Ty1 particles are apparently more structurally heterogeneous than Ty3 VLPs, expression of truncated (e.g., 1 to 346 and 1 to 408 aa) and full-length (1 to 440 aa) *TYA* results in production of more homogeneous particles. These have been studied by transmission electron microscopy and cEM (1). That study concluded that the length of *TYA* expressed correlated with particle size and also with icosahedral class (1). However, this conclusion is complicated by the fact that particles of more than one T number were reported assembled within cells expressing individual protein constructs. Particles produced by aa 1 to 346 were T=3 and T=4; aa 1 to 408 (p2) were T=4 and T=7; and aa 1 to 440 (p1 protein) were T=7 and T=9. Relatively fewer T=7 and T=9 particles were available for analysis. While the reason for this is not clear, it could similarly be the case for Ty3 that the broad distribution of particle sizes reflects subpopulations of truncated or degraded structural protein with representation of different sizes controlled by the kinetics of assembly.

Although the heterogeneity of particle sizes for Ty3 wt, PR, and RT mutants could be explained as described above for Ty1, the size distribution of the PR and the RT mutant VLPs caused us to favor the third explanation, that a significant number of particles of smaller diameters correspond to particles at different stages in the Ty3 life cycle during or after reverse transcription. If Ty3 CA were rearranged during or subsequent to reverse transcription, then the smaller particles would be derived from the larger particles. This would not necessarily preclude the possibility that both large and small particles possess icosahedral symmetry. Although it may seem surprising that icosahedral structure could be maintained through such a transition, T=3 to T=1 transformations have been observed for southern bean mosaic, sesbania mosaic, alfalfa mosaic, and brome mosaic viruses which lose hexagonal capsomeres during the process (47). Alternatively, it could be that the particles undergo partial or complete disassembly and reformation associated with reverse transcription. Recent three-dimensional structural analysis of HIV VLPs using electron cryotomography showed enveloped structures containing multiple capsids and nested capsids which were interpreted as incompatible with a concerted condensation model but rather suggestive of a de novo reassembly process (3).

The ratio of volumes for icosahedra of T=7, 4, and 3 composed of the same capsid protein are 1:0.432:0.281 (35). From this it appears that particles in the T=4 and T=3 size range would also be relatively restricted in the amount of nucleic acid they could contain and that one or both might in fact be empty. Although we cannot exclude the possibility that production of T=3 and 4 particles is suppressed or defective in cells expressing the PR and RT mutants, the simplest interpretation of our data is that smaller structured particles form as a result of some process associated with reverse transcription or subsequent stage of morphogenesis.

The yeast nuclear pore is estimated to accommodate particles ranging up to 30 nm (51). Thus, Ty3 cDNA would probably be associated with some complex different than the T=7 VLPs we have described in order to transit the nuclear pore. In the case of at least a few retroviruses, including HIV-1, several types of data suggest that reverse transcription is associated

with disintegration or uncoating of the core particle (20, 56, 61). For others, such as spuma viruses, where the incoming particle is observed in the nuclear periphery (50, 68), cDNA synthesis may be delayed or may not be accompanied by particle disintegration. The Ty3 wt VLP fraction that we examined in this study has in vitro integration activity (39), and analysis of the sucrose gradient fractions for cDNA indicates that Ty3 cDNA is found in this interface fraction (28). However, the amount of cDNA found near the top of the gradient is significantly greater (unpublished data) than that found in the interface fraction. Investigation of the upper portions of the gradient by AFM was impeded by a very high background of cellular material unrelated to Ty3 (data not shown).

Yeast retrotransposons assemble into particles analogous to mature retrovirus cores. We propose that retrotransposons which assemble within the cytoplasm bypass the external particle remodeling characteristic of retrovirus cores and assemble directly into a form externally similar to the subsequent mature structure. Both mature retrovirus cores and retrotransposon VLPs display the structural features of icosahedral organization. Using AFM, we were able to image both pentameric and hexameric capsomeres on the surfaces of individual Ty3 core particles. We believe that this represents the first direct visualization of such features in a retrovirus or retrotransposon particle. Ty3 VLPs are in many ways similar to retrovirus capsids and may represent a good model for their structure and assembly. Both are constructed according to icosahedral symmetry or derived from it by a redistribution of capsomeres or the introduction of defects. Hence, the structural features we observe on the Ty3 particles may reflect corresponding properties of those retroviral capsids.

ACKNOWLEDGMENTS

This research was supported by Public Health Services grant GM58868 from the National Institutes of Health to A.M.; Public Health Services Grant GM33281 to S.B.S.; and National Science Foundation Grant 9983116 to T.M.M. M.Z. was supported in part by a grant from the UC Biotechnology Research and Education Program.

We thank A. Greenwood for his assistance with the preparation of figures and S. Larson and L. Larsen for helpful discussions. We thank D. Lener and S. LeGrice (NCI, Frederick, MD) for providing the Ty3 RT mutant (D213N) plasmid. We thank S. Moore and D. Garfinkel (NCI, Frederick, MD) for providing rabbit polyclonal anti-TYA protein antibody and Ty1 VLP standards.

REFERENCES

1. **Al Khayat, H. A., D. Bhella, J. M. Kenney, J. F. Roth, A. J. Kingsman, E. Martin-Rendon, and H. R. Saibil.** 1999. Yeast Ty retrotransposons assemble into virus-like particles whose T-numbers depend on the C-terminal length of the capsid protein. J. Mol. Biol. **292:**65–73.
2. **Ausubel, F. M., R. Brent, R. E. Kingston, D. D. Moore, J. G. Seidman, J. A. Smith, and K. Struhl.** 1999. Current protocols in molecular biology. Greene Publishing Associates/Wiley-Interscience, New York, N.Y.
3. **Benjamin, J., B. K. Ganser-Pornillos, W. F. Tivol, W. I. Sundquist, and G. J. Jensen.** 2005. Three-dimensional structure of HIV-1 virus-like particles by electron cryotomography. J. Mol. Biol. **346:**577–588.
4. **Bilanchone, V. W., J. A. Claypool, P. T. Kinsey, and S. B. Sandmeyer.** 1993. Positive and negative regulatory elements control expression of the yeast retrotransposon Ty3. Genetics **134:**685–700.
5. **Boeke, J. D., T. H. Eickbush, S. B. Sandmeyer, and D. F. Voytas.** 2000. Metaviridae *In* M. H. V. van Regenmortel, C. M. Fauquet, D. H. L. Bishop, E. B. Carsten, M. K. Estes, S. M. Lemon, J. Maniloff, M. A. Mayo, D. J. McGeoch, C. R. Pringle, and R. B. Wickner (ed.), Virus taxonomy: seventh report of the International Committee on Taxonomy of Viruses. Academic Press, New York, N.Y.
6. **Bradford, M. M.** 1976. A rapid and sensitive method for the quantitation of microgram quantities of protein utilizing the principle of protein dye binding. Anal. Biochem. **72:**248–254.
7. **Briggs, J. A. G., M. N. Simon, I. Gross, H. G. Krausslich, S. D. Fuller, V. M. Vogt, and M. C. Johnson.** 2004. The stoichiometry of Gag protein in HIV-1. Nat. Struct. Mol. Biol. **11:**672–675.
8. **Briggs, J. A. G., B. E. Watson, B. E. Gowen, and S. D. Fuller.** 2004. Cryo-electron microscopy of mouse mammary tumor virus. J. Virol. **78:**2606–2608.
9. **Briggs, J. A. G., T. Wilk, R. Welker, H. G. Krausslich, and S. D. Fuller.** 2003. Structural organization of authentic, mature HIV-1 virions and cores. EMBO J. **22:**1707–1715.
10. **Burns, N. R., H. R. Saibil, N. S. White, J. F. Pardon, P. A. Timmins, S. Mark, H. Richardson, B. M. Richards, S. E. Adams, S. M. Kingsman, and A. J. Kingsman.** 1992. Symmetry, flexibility and permeability in the structure of yeast retrotransposon virus-like particles. EMBO J. **11:**1155–1164.
11. **Burstein, H., D. Bizub, and A. M. Skalka.** 1991. Assembly and processing of avian retroviral Gag polyproteins containing linked protease dimers. J. Virol. **65:**6165–6172.
12. **Caspar, D. L. D., and A. Klug.** 1962. Physical principles in construction of regular viruses. Cold Spring Harb. Symp. Quant. Biol. **27:**1–22.
13. **Coffin, J. M., S. H. Hughes, and H. E. Varmus (ed.).** 1997. Retroviruses. Cold Spring Harbor Laboratory Press, Plainview, N.Y.
14. **Craig, N., R. Craigie, M. Gellert, and A. M. Lambowitz (ed.).** 2002. Mobile DNA II. ASM Press, Washington, D.C.
15. **Craven, R. C., A. E. Leure-DuPree, Jr., R. A. Weldon, and J. W. Wills.** 1995. Genetic analysis of the major homology region of the Rous sarcoma virus Gag protein. J. Virol. **69:**4213–4227.
16. **Curcio, M. J., and D. J. Garfinkel.** 1992. Posttranslational control of Ty1 retrotransposition occurs at the level of protein processing. Mol. Cell. Biol. **12:**2813–2825.
17. **Elder, R. T., T. P. St. John, D. T. Stinchcomb, and R. W. Davis.** 1981. Studies on the transposable element Ty1 of yeast. I. RNA homologous to Ty1. Cold Spring Harb. Symp. Quant. Biol. **45:**581–584.
18. **Farabaugh, P. J., H. Zhao, S. Pande, and A. Vimaladithan.** 1993. Translational frameshifting expresses the *POL3* gene of retrotransposon Ty3 of yeast. Cell **74:**93–103.
19. **Flint, S., L. Enquist, V. Racaniello, and A. Skalka.** 2004. Principles of virology. ASM Press, Washington, D.C.
20. **Forshey, B. M., U. von Schwedler, W. I. Sundquist, and C. Aiken.** 2002. Formation of a human immunodeficiency virus type 1 core of optimal stability is crucial for viral replication. J. Virol. **76:**5667–5677.
21. **Fuller, S. D., T. Wilk, B. E. Gowen, H. G. Krausslich, and V. M. Vogt.** 1997. Cryo-electron microscopy reveals ordered domains in the immature HIV-1 particle. Curr. Biol. **7:**729–738.
22. **Gamble, T. R., F. F. Vajdos, S. H. Yoo, D. K. Worthylake, M. Houseweart, W. I. Sundquist, and C. P. Hill.** 1996. Crystal structure of human cyclophilin A bound to the amino-terminal domain of HIV-1 capsid. Cell **87:**1285–1294.
23. **Ganser, B. K., A. C. Cheng, W. I. Sundquist, and M. Yeager.** 2003. Three-dimensional structure of the M-MuLV CA protein on a lipid monolayer: a general model for retroviral capsid assembly. EMBO J. **22:**2886–2892.
24. **Ganser, B. K., S. Li, V. Y. Klishko, J. T. Finch, and W. I. Sundquist.** 1999. Assembly and analysis of conical models for the HIV-1 core. Science **283:**80–83.
25. **Garfinkel, D. J., J. D. Boeke, and G. R. Fink.** 1985. Ty element transposition: reverse transcriptase and virus-like particles. Cell **42:**507–517.
26. **Gitti, R. K., B. M. Lee, J. Walker, M. F. Summers, S. Yoo, and W. I. Sundquist.** 1996. Structure of the amino-terminal core domain of the HIV-1 capsid protein. Science **273:**231–235.
27. **Gross, I., H. Hohenberg, T. Wilk, K. Wiegers, M. Grattinger, B. Muller, S. Fuller, and H. G. Krausslich.** 2000. A conformational switch controlling HIV-1 morphogenesis. EMBO J. **19:**103–113.
28. **Hansen, L. J., D. L. Chalker, K. J. Orlinsky, and S. B. Sandmeyer.** 1992. Ty3 *GAG3* and *POL3* genes encode the components of intracellular particles. J. Virol. **66:**1414–1424.
29. **Hansen, L. J., D. L. Chalker, and S. B. Sandmeyer.** 1988. Ty3, a yeast retrotransposon associated with tRNA genes, has homology to animal retroviruses. Mol. Cell. Biol. **8:**5245–5256.
30. **Hansma, H. G., K. A. Browne, M. Bezanilla, and T. C. Bruice.** 1994. Bending and straightening of DNA induced by the same ligand - characterization with the atomic-force microscope. Biochemistry **33:**8436–8441.
31. **Hansma, H. G., and J. H. Hoh.** 1994. Biomolecular imaging with the atomic-force microscope. Annu. Rev. Biophys. Biomol. Struct. **23:**115–139.
32. **Harrison, S. C.** 1990. Principles of virus structure, p. 37–61. *In* B. N. Fields and D. Knipe (ed.), Virology. Raven Press, New York, N.Y.
33. **Jaspars, E. M. J.** 1985. Interaction of alfalfa mosaic virus nucleic acid and protein, p. 155–221. *In* J. W. Davies (ed.), Molecular plant virology. CRC Press, Inc., Boca Raton, Fla.
34. **Joshi, S. M., and V. M. Vogt.** 2000. Role of the rous sarcoma virus p10 domain in shape determination of Gag virus-like particles assembled in vitro and within *Escherichia coli*. J. Virol. **74:**10260–10268.
35. **Jurnak, F. A., and A. McPherson.** 1984. Biological macromolecules and assemblies, virus structures, p. 225–299. **(ed.)**. John Wiley, New York, N.Y.
36. **Kaper, J. M.** 1975. The Chemical Basis of virus structure, dissociation and reassembly. North Holland Publishing Co., Amsterdam, The Netherlands.
37. **Kingston, R. L., T. Fitzon-Ostendorp, E. Z. Eisenmesser, G. W. Schatz, V. M.**

Vogt, C. B. Post, and M. G. Rossmann. 2000. Structure and self-association of the Rous sarcoma virus capsid protein. Struct. Fold. Design **8:**617–628.
38. **Kingston, R. L., N. H. Olson, and V. M. Vogt.** 2001. The organization of mature Rous sarcoma virus as studied by cryoelectron microscopy. J. Struct. Biol. **136:**67–80.
39. **Kirchner, J., C. M. Connolly, and S. B. Sandmeyer.** 1995. Requirement of RNA polymerase III transcription factors for *in vitro* position-specific integration of a retroviruslike element. Science **267:**1488–1491.
40. **Kirchner, J., and S. B. Sandmeyer.** 1993. Proteolytic processing of Ty3 proteins is required for transposition. J. Virol. **67:**19–28.
41. **Kirchner, J., S. B. Sandmeyer, and D. B. Forrest.** 1992. Transposition of a Ty3 *GAG3-POL3* fusion mutant is limited by availability of capsid protein. J. Virol. **66:**6081–6092.
42. **Kuznetsov, Y., G. Yu, J. R. Gurnon, J. L. Van Etten, and A. McPherson.** 2005. Atomic force microscopy investigation of a chlorella virus, PBCVB-1. J. Struct. Biol. **149:**256–263.
43. **Kuznetsov, Y. G., S. Datta, N. H. Kothari, A. Greenwood, H. Fan, and A. McPherson.** 2002. Atomic force microscopy investigation of fibroblasts infected with wild-type and mutant murine leukemia virus. Biophys. J. **83:** 3665–3674.
44. **Kuznetsov, Y. G., A. J. Malkin, R. W. Lucas, M. Plomp, and A. McPherson.** 2001. Imaging of viruses by atomic force microscopy. J. Gen. Virol. **82:** 2025–2034.
45. **Kuznetsov, Y. G., J. G. Victoria, W. E. Robinson, and A. McPherson.** 2003. Atomic force microscopy investigation of human immunodeficiency virus (HIV) and HIV-infected lymphocytes. J. Virol. **77:**11896–11909.
46. **Kyte, J., and R. F. Doolittle.** 1982. A simple method for displaying the hydropathic character of a protein. J. Mol. Biol. **157:**105–132.
47. **Larson, S. B., R. W. Lucas, and A. McPherson.** 2005. Crystallographic structure of the T=1 particle of brome mosaic virus. J. Mol. Biol. **346:**815–831.
48. **Levin, H. L.** 2002. Newly identified retrotransposons of the Ty3/gypsy class in fungi, plants, and vertebrates, p. 684–701. *In* N. L. Craig, R. Craigie, M. Gellert, and A. M. Lambowitz (ed.), Mobile DNA II. ASM Press, Washington, D.C.
49. **Li, S., C. P. Hill, W. I. Sundquist, and J. T. Finch.** 2000. Image reconstructions of helical assemblies of the HIV-1 CA protein. Nature **407:**409–413.
50. **Linial, M. L., and S. W. Eastman.** 2003. Particle assembly and genome packaging. Foamy Vir. **277:**89–110.
51. **Macara, I. G.** 2001. Transport into and out of the nucleus. Microbiol. Mol. Biol. Rev. **65:**570–594.
52. **Malkin, A. J., Y. G. Kuznetsov, R. W. Lucas, and A. McPherson.** 1999. Surface processes in the crystallization of turnip yellow mosaic virus visualized by atomic force microscopy. J. Struct. Biol. **127:**35–43.
53. **MartinRendon, E., D. W. Hurd, G. Marfany, S. M. Kingsman, and A. J. Kingsman.** 1996. Identification of proteolytic cleavage sites within the gag-analogue protein of Ty1 virus-like particles. Mol. Microbiol. **22:**1035–1043.
54. **Mayo, K., M. L. Vana, J. McDermott, D. Huseby, J. Leis, and E. Barklis.** 2002. Analysis of Rous sarcoma virus capsid protein variants assembled on lipid monolayers. J. Mol. Biol. **316:**667–678.
55. **McDermott, J., K. Mayo, and E. Barklis.** 2000. Three-dimensional organization of retroviral capsid proteins on a lipid monolayer. J. Mol. Biol. **302:** 121–133.
56. **McDonald, D., M. A. Vodicka, G. Lucero, T. M. Svitkina, G. G. Borisy, M. Emerman, and T. J. Hope.** 2002. Visualization of the intracellular behavior of HIV in living cells. J. Cell Biol. **159:**441–452.
57. **Menees, T. M., and S. B. Sandmeyer.** 1994. Transposition of the yeast retroviruslike element Ty3 is dependent on the cell cycle. Mol. Cell. Biol. **14:** 8229–8240.
58. **Merkulov, G. V., K. M. Swiderek, C. Baker Brachmann, and J. D. Boeke.** 1996. A critical proteolytic cleavage site near the C terminus of the yeast retrotransposon Ty1 Gag protein. J. Virol. **70:**5548–5556.
59. **Momany, G., L. C. Kovari, A. J. Prongay, W. Keller, R. K. Gitti, B. M. Lee, A. E. Gorbalenya, L. Tong, J. McClure, L. S. Ehrlich, M. F. Summers, C. Carter, and M. G. Rossmann.** 1996. Crystal structure of dimeric HIV-1 capsid protein. Nat. Struct. Biol. **3:**763–770.
60. **Mortuza, G. B., L. F. Haire, A. Stevens, S. J. Smerdon, J. P. Stoye, and I. A. Taylor.** 2004. High-resolution structure of a retroviral capsid hexameric amino-terminal domain. Nature **431:**481–485.
61. **Nermut, M. V., and A. Fassati.** 2003. Structural analyses of purified human immunodeficiency virus type 1 intracellular reverse transcription complexes. J. Virol. **77:**8196–8206.
62. **Nermut, M. V., D. J. Hockley, P. Bron, D. Thomas, W. H. Zhang, and I. M. Jones.** 1998. Further evidence for hexagonal organization of HIV gag protein in prebudding assemblies and immature virus-like particles. J. Struct. Biol. **123:**143–149.
63. **O'Connell, K. L., and J. T. Stults.** 1997. Identification of mouse liver proteins on two-dimensional electrophoresis gels by matrix-assisted laser desorption ionization mass spectrometry of in situ enzymatic digests. Electrophoresis **18:** 349–359.
64. **O'Farrell, P. H.** 1975. High resolution two-dimensional electrophoresis of proteins. J. Biol. Chem. **250:**4007–4021.
65. **Orlinsky, K., J. Gu, M. Hoyt, S. Sandmeyer, and T. Menees.** 1996. Mutations in the Ty3 major homology region affect viruslike particle morphogenesis. J. Virol. **70:**3440–3448.
66. **Orlinsky, K. J., and S. B. Sandmeyer.** 1994. The Cys-His motif of Ty3 NC can be contributed by Gag3 or Gag3-Pol3 polyproteins. J. Virol. **68:**4152–4166.
67. **Palmer, K. J., W. Tichelaar, N. Myers, N. R. Burns, S. J. Butcher, A. J. Kingsman, S. D. Fuller, and H. R. Saibil.** 1997. Cryo-electron microscopy structure of yeast Ty retrotransposon virus-like particles. J. Virol. **71:**6863–6868.
68. **Petit, C., M. L. Giron, J. Tobaly-Tapiero, P. Bittoun, E. Real, Y. Jacob, N. Tordo, H. de The, and A. Saib.** 2003. Targeting of incoming retroviral Gag to the centrosome involves a direct interaction with the dynein light chain 8. J. Cell Sci. **116:**3433–3442.
69. **Pettit, S. C., M. D. Moody, R. S. Wehbie, A. H. Kaplan, P. V. Nantermet, C. A. Klein, and R. Swanstrom.** 1994. The P2 Domain of Hum.-Immunodeficiency-virus type-1 Gag regulates sequential proteolytic processing and is required to produce fully infectious virions. J. Virol. **68:**8017–8027.
70. **Pettit, S. C., J. Simsic, D. D. Loeb, L. Everitt, C. A. Hutchison III, and R. Swanstrom.** 1991. Analysis of retroviral protease cleavage sites reveals two types of cleavage sites and the structural requirements of the P1 amino acid. J. Biol. Chem. **266:**14539–14547.
71. **Rausch, J. W., M. K. Le Grice, M. H. Nymark-McMahon, J. T. Miller, and S. F. LeGrice.** 2000. Interaction of p55 reverse transcriptase from the Saccharomyces cerevisiae retrotransposon Ty3 with conformationally distinct nucleic acid duplexes. J. Biol. Chem. **275:**13879–13887.
72. **Rayment, I.** 1984. Animal virus structure, p. 255–298. *In* F. A. Jurnak and A. McPherson (ed.), Biological macromolecules and assemblies. John Wiley, New York, N.Y.
73. **Rossmann, M. G., and J. W. Erickson.** 1985. Structure and assembly of icosahedral shells, p. 29–74. *In* S. Casjens (ed.), Virus structure and assembly. Jones and Bartlett Publishing, Inc., Boston, Mass.
74. **Roth, J. F.** 2000. The yeast Ty virus-like particles. Yeast **16:**785–795.
75. **Sandmeyer, S. B., M. Aye, and T. M. Menees.** 2002. Ty3: a position-specific, gypsylike element in *Saccharomyces cerevisiae*, p. 663–682. *In* N. L. Craig, R. Craigie, M. Gellert, and A. M. Lambowitz (ed.), Mobile DNA II. ASM Press, Washington, D.C.
76. **Scarlata, S., and C. Carter.** 2003. Role of HIV-1 Gag domains in viral assembly. Biochim. Biophys. Acta-Biomembranes **1614:**62–72.
77. **van Regenmortel, M., C. Fauquet, and D. H. L. Bishop (ed.)** 2000. Virus taxonomy. Academic Press, New York, N.Y.
78. **Vogt, V. M.** 1996. Proteolytic processing and particle maturation. Curr. Top. Microbiol. Immunol. **214:**95–131.
79. **Vogt, V. M.** 1997. Retroviral virions and genomes, p. 27–69. *In* J. M. Coffin, S. H. Hughes, and H. E. Varmus (ed.), Retroviruses. Cold Spring Harbor Laboratory Press, Plainview, N.Y.
80. **von Schwedler, U. K., T. L. Stemmler, V. Y. Klishko, S. Li, K. H. Albertine, D. R. Davis, and W. I. Sundquist.** 1998. Proteolytic refolding of the HIV-1 capsid protein amino-terminus facilitates viral core assembly. EMBO J. **17:** 1555–1568.
81. **Voytas, D. F., and J. D. Boeke.** 2002. Ty1 and Ty5 of *Saccharomyces cerevisiae*, p. 631–683. *In* N. Craig, R. Craigie, M. Gellert, and A. M. Lambowitz (ed.), Mobile DNA II. ASM Press, Washington, D.C.
82. **Wilk, T., and S. D. Fuller.** 1999. Towards the structure of the human immunodeficiency virus: divide and conquer? Curr. Opin. Cell Biol. **9:**231–243.
83. **Wilk, T., B. Gowen, and S. D. Fuller.** 1999. Actin associates with the nucleocapsid domain of the human immunodeficiency virus Gag polyprotein. J. Virol. **73:**1931–1940.
84. **Wilk, T., I. Gross, B. E. Gowen, T. Rutten, F. de Haas, R. Welker, H. G. Krausslich, P. Boulanger, and S. D. Fuller.** 2001. Organization of immature human immunodeficiency virus type 1. J. Virol. **75:**759–771.
85. **Winston, F., K. J. Durbin, and G. R. Fink.** 1984. The *SPT3* gene is required for normal transcription of Ty elements in *S. cerevisiae*. Cell **39:**657–682.
86. **Yeager, M., E. M. Wilson-Kubalek, S. G. Weiner, P. O. Brown, and A. Rein.** 1998. Supramolecular organization of immature and mature murine leukemia virus revealed by electron cryo-microscopy: implications for retroviral assembly mechanisms. Proc. Natl. Acad. Sci. USA **95:**7299–7304.
87. **Youngren, S. D., J. D. Boeke, N. J. Sanders, and D. J. Garfinkel.** 1988. Functional organization of the retrotransposon Ty from *Saccharomyces cerevisiae*: Ty protease is required for transposition. Mol. Cell. Biol. **8:**1421–1431.
88. **Yu, F., S. M. Joshi, Y. M. Ma, R. L. Kingston, M. N. Simon, and V. M. Vogt.** 2001. Characterization of Rous sarcoma virus Gag particles assembled in vitro. J. Virol. **75:**2753–2764.
89. **Zhou, J., X. Yuan, D. Dismuke, B. M. Forshey, C. Lundquist, K. H. Lee, C. Aiken, and C. H. Chen.** 2004. Small-molecule inhibition of human immunodeficiency virus type 1 replication by specific targeting of the final step of virion maturation. J. Virol. **78:**922–929.
90. **Zuber, G., and E. Barklis.** 2000. Atomic force microscopy and electron microscopy analysis of retrovirus gag proteins assembled in vitro on lipid bilayers. Biophys. J. **78:**373–384.
91. **Zuber, G., J. McDermott, S. Karanjia, W. Y. Zhao, M. F. Schmid, and E. Barklis.** 2000. Assembly of retrovirus capsid-nucleocapsid proteins in the presence of membranes or RNA. J. Virol. **74:**7431–7441.